Antenna Design and Measurements for Conductive Thermal Transfer Printing Based RFID Production

Ishita Dhopeshwar[1], Maxwell McManus[1], Dan Harrison[2], Betty Ralston[2],
Christopher Janson[3], Alan Rae[3], Adrian Levesque[3], and Zhangyu Guan[1]

[1]Department of Electrical Engineering, University at Buffalo, Buffalo, NY 14260, USA

[2]ARMOR-IIMAK, Buffalo, Amherst, NY, 14228

[3]Center of Excellence in Material Informatics (CMI), University at Buffalo, Buffalo, NY 14260, USA

Abstract—In this article we present a new RFID antenna design based on conductive thermal transfer printing. We first describe the key antenna design parameters, including antenna shape, dimensions, and number of lobes, among others. The desirable range of these parameters have been determined empirically through an extensive experimentation campaign for impedance matching. Then, we print the antenna using conductive Aluminum ribbon on PET coated paper. We evaluate the performance of the new antenna by comparing it with 13 existing benchmark antennas using a commercial RFID reader at 915 MHz. It is found that the new antenna design can achieve better range-angle trade-off than the benchmarks.

Index Terms—RFID, Antenna Design, Impedance Matching, Conductive Thermal Transfer Printing.

I. INTRODUCTION

Radio frequency identification (RFID) technology has become a ubiquitous technology with well-defined applications across a diverse and expansive set of industries such as commerce [1], inventory management [2], and healthcare [3], among many others. In general, an RFID system is comprised of a reader, which is an RF transceiver unit with some data processing, and a tag, which is a chip containing programmable internal memory interfaced with an antenna element [4]. The reader will first emit an RF signal, which is received by the tag. The received signal energy is used to passively generate a backscatter signal, which is modulated using information from the chip internal memory. The backscatter signal is then detected by the reader and demodulated to recover the information provided by the tag.

The widespread adoption of RFID has drawn significant research interest over the past decade towards antenna design and tag manufacturing methods [5]. Among these new tag design methods includes conductive thermal transfer printing, which has been envisioned as a key technology that can enable rapid and distributed RFID production. Aided by flexible conductive ribbon, this technology can thermally transfer (or print) conductive materials to substrates like paper and Polyethylene terephthalate (PET) with high precision. Using this method, many antennas can be printed rapidly using low-cost materials, compared to other fabrication methods such as laser etching [6] which are more expensive to establish and maintain.

While many new RFID design practices have shown promise in existing literature, the commercial adoption of new technologies such as thermal transfer printing for RFID remains an open question. A primary challenge is in the lack of flexible and scalable RFID antenna prototyping methods, based on which new RFID tags can be manufactured with optimized performance under specific manufacturing constraints such as ribbon substrate, printing method, and chip placement technique, among others. To address this challenge, in this article we explore thermal transfer printing technology for the design of new passive RFID antennas, and demonstrate performance of these tags in relation to various design considerations. In the rest of this article, we first discuss the related works in Section II, and then describe the antenna design approach in Section III. In Section IV we describe the RFID prototyping method and we present and discuss the performance evaluation results in Section V. Finally, we draw the main conclusions and discuss the future work in Section VI. *The joint work presented in this paper, conducted by the University at Buffalo and ARMOR-IIMAK Corporation, is the subject of a pending patent application filed with the United States Patent Office on January 19, 2023.*

II. RELATED WORK

The RFID tag design process is based on a set of application-specific criteria, which can be translated to physical constraints to inform antenna design. The authors of [7] discuss and explain the basic RFID chip development technique, focusing on how to configure factors such as size, layout, and orientation to meet the demands of various industrial applications. In [8], the authors discuss basic concepts of tag design and printing for popular commercial designs and emphasize the importance of matched impedance for design validation. In [9]–[11], the concept of meander line is discussed as an impedance matching technique for tag development. The authors of [10] propose a new meander line technique to optimize the overall antenna gain, interpreting meander lines as transmission lines which affect the global antenna impedance. The authors of [9] incorporate loading bars into the antenna design to facilitate impedance matching without adjusting the antenna dimensions, improving design flexibility under application-specific constraints. The authors of [11] demonstrate the meander line design technique for impedance matching on electrically short ($< 1/4\lambda$) antennas for use in frequency ranges below 30 MHz. The authors of [12] investigate a multiple-antenna reader design for inventory

management and localization for use with passive UHF tags. The authors of [13] design and test an analog RFID tag using an open-circuit design with L-shape stubs. In [14], the authors characterize a dipole antenna using S-parameters, port extension, and de-embedding to accelerate the design process. The authors of [14] also discuss the use of ANSYS High Frequency Structure Simulator (HFSS) [15] to accelerate the RFID design process.

Antenna impedance measurement is a very important step during tag design with significant impact on the efficiency of the backscatter signal response hence read range of the tag. In [16], Cai et al. discuss three different methods of RFID antenna impedance measurement, including Balun, image processing, and S-parameter methods, and demonstrate both simulation and prototype results for each. The authors of [17] discuss the impedance measurement techniques using a Vector Network Analyzer (VNA), explaining calibration techniques to ensure maximum accuracy. In [18], the authors provide a guideline for understanding the basics of antenna and backscatter signals. The authors of [19] discuss the use of an artificial magnetic conductor inserted between the antenna and the chip for mm-wave ASICs.

The RFID antenna fabrication method is a key consideration which must be considered during the tag design process to enable large-scale production. The authors of [20] demonstrate the use of inkjet printing to test a bowtie antenna design for use in the UHF band, and achieve a read range of 3.8 meters. The authors of [20] also discuss the inkjet tag design process, proposing a T-match shape of the inner loop to reduce the return loss of the antenna. Gigac et al. [21] demonstrate the advantages of thermal printing over inkjet printing considering different substrates for various designs. The authors of [6] demonstrate the use of laser-cut gold attached to PET to compare chipless tag designs for wearable applications. The authors of [22] show the performance of UHF tags designed to be embroidered into surgical masks The authors of [23] leverage 3-D printing techniques such as fused filament fabrication, aerosol jet printing, and laser-induced graphene to generate conductive elements for UHF tags. The authors of [24] also leverage 3-D printing techniques to design a miniaturized "antenna-in-package" tag measuring less than 16.5 mm in all dimensions for use in the UHF band. In [25], the authors use HFSS to develop and test different bow tie antennas, and evaluate using printed aluminum on polyethylene naphthalate (PEN). The authors of [26] provide a detailed discussion of the development and measurement of several different tag designs for underground RFID systems. *In this work, we design new RFID antennas based on thermal transfer printing technology with conductive Aluminum ribbon and test the resulting RFID tags against numerous commercial designs.*

III. Antenna Design Approach

A. RFID: A Primer

A passive RFID system is typically comprised of a reader, comprised of a transceiver module and a processing unit, and series of tags, comprised of antenna elements connected to integrated circuits, or "chips". The reader will send out a control signal to request data from the tag, typically in the UHF band, and the tag will generate a radiated "backscatter" signal using the energy from that control signal. This control signal can either contain information to write to the chip memory, or can simply be used to induce a response from the tag. The backscatter signal is modulated by the application specific chip, which is activated when exposed to the current generated by the received control signal. The radiated signal power, typically in the range of -25 to -40 dBW, is determined by the current distribution of the collected energy from the control signal, as well as the impedance matching between the antenna and chip. Next we describe the key design parameters of the proposed new RFID antenna.

B. Antenna Design Parameters

As introduced in Section I, we aim to design novel antennas with optimized read range and angle using the thermal transfer printing method. In order to design new antennas and compare them with existing commercial antenna designs, we first identify several key design parameters to demonstrate the relationship between antenna geometry and overall tag performance. These parameters, which are illustrated in Figure 1, are defined as follows, along with the respective ranges considered in this work:

- *Reference Line:* This is the horizontal line for demonstrating tag rotation relative to reader orientation.
- *Antenna Length d_{ant}:* This is the antenna length measured along reference line axis (7 - 11 cm)
- *Antenna Height h_{ant}:* This is antenna height measured perpendicular to reference line axis (1 - 5 cm).
- *Inner Loop Dimension d_{in}:* This is the inner diameter of loop connecting antenna lobes to chip box (0.8 - 3 cm).
- *Outer Loop Dimension d_{out}:* This is the outer diameter of loop connecting antenna lobes to chip box (0.1 - 4 cm).
- *Loop Thickness t_{in}:* This defines the minimum thickness of loop connecting antenna lobes to chip box, defined as $t_{in} := d_{out} - d_{in}$ for all antenna designs.
- *Lobe Length l:* This defines the length from outer loop boundary to end of longest lobe (2.5 - 4.5 cm).
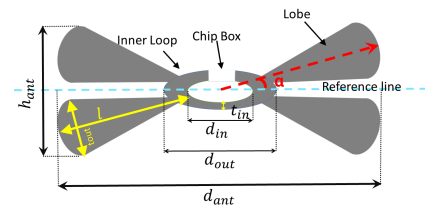
Fig. 1: Illustration of antenna design parameters on antenna Ant-2-100-15-35.
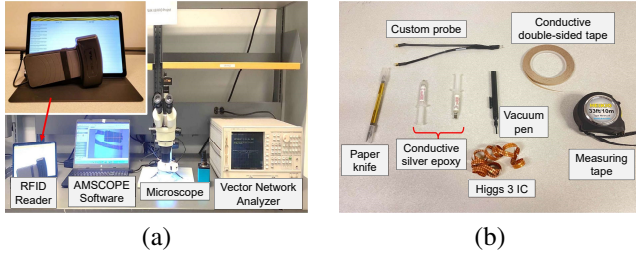
Fig. 2: Tools and facilities for RFID tag fabrication. (a) Lab setup (from left): RFID Reader TURCK, laptop with AMSCOPE software, AMSCOPE FMA050 microscope, vector network analyzer (VNA); (b) tools required for tag fabrication.

- *Lobe Thickness* t_{out}: This represents the maximum width of each lobe in the antenna (0.8 - 1 cm).
- *Lobe Angle* α: This is the maximum angle between the outermost lobe and the reference line, varying with n_l in the range of 0° ($n_l = 1$) to 90° ($n_l = 5$).
- *Chip Box* This is the loop separation for chip placement, which determines the width of the air cavity under the chip and, set to 0.45 mm or 8 mm in this work.

A five-field naming method "Ant-n_l-d_{ant}-h_{ant}-α" is used, where the first field "Ant" is short for Antenna, the second field indicates the number of lobes n_l, the third represents the antenna width d_{ant}, the fourth field is the height of the antenna h_{ant}, and the last field corresponds to the angle of the lobes α. For clarity, the last field is omitted in cases where $n_l = 1$ or in cases where there are multiple possible values of α. In general, we reference to the thickness t_{out} of the lobe rather than h_{ant}, however for Ant-1-d_{ant}-h_{ant}, the value of t_{out} and h_{ant} is the same.

In this work we propose a new antenna design with a symmetrical multi-lobe shape, in which the chip box is an enclosed loop. Based on extensive prototyping and experimentation, we select the symmetrical lobe shape with increasing dimensions moving away from the chip, as shown in Figure 1. We generate twenty antenna designs using this methodology as shown in Figure 4. In general, the length of the antenna along the reference line axis d_{ant} should be greater than or equal to a fourth of the wavelength λ i.e. $d_{ant} \geq \lambda/4$ [27], [28], which for UHF tag at 915 MHz can be approximated to 8.25 cm. Using this design, we determine the value of other geometric parameters by matching the impedance of the antenna to that of the IC and analyzing the relationship between antenna geometry and current distribution. We discuss this further in Sections IV and V. Furthermore, we show that, by increasing the number of lobes n_l, lobe angle α, and tag height h_aant, we can provide an improved read range at higher orientation angle β.

IV. RFID TAG PROTOTYPING

In order to investigate the optimal tag performance for thermal transfer printing, we design an experimental campaign to explore numerous RFID antenna designs, focusing on the relationship between the parameters outlined in Section III
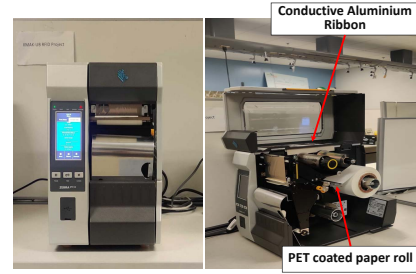
Fig. 3: ZT610 printer: (left) front view and (right) inside view.

and both read range and read angle performance. We use a commercial handheld RFID reader at an operational frequency range of 865-915 MHz. As mentioned in Section III, this frequency range determines the desired major-axis dimension (to be identified in this work) of the printed RFID tags. In all cases, we fabricate the antennas used in this investigation using the thermal transfer printing method, selecting aluminum ribbon as our antenna material and PET as the printing substrate. This enables rapid, scalable manufacture of all printed antennas in this investigation.

Current Distribution and Radiation Pattern. The antenna designs are first investigated using the MATLAB Partial Differential Equations (PDE) and Antenna Design toolboxes. First, the antenna geometry is defined in MATLAB based on each design. A triangle mesh is fit to the antenna geometry using a maximum edge length of 2 mm, and the current distribution is simulated based on this mesh. It is found that a uniform current distribution across the antenna surface corresponds to improved backscatter signal strength hence good read range, while high variance in the current distribution leads to poor performance overall.

Using the Antenna Design Toolbox, the antenna radiation pattern and the impedance across the chip box are calculated based on the current distribution. These metrics provide an estimate of the antenna's read range and angle. Mismatched impedance between the antenna and the chip lowers the tag's energy efficiency, resulting in a lower backscatter signal power hence reduced read range. Antennas with a highly directional radiation pattern, such as Ant-1-100-10, demonstrate a very high read range but with poor performance at $\beta > 0°$, while antennas with a more isotropic radiation pattern demonstrate lower maximum read range but with good performance
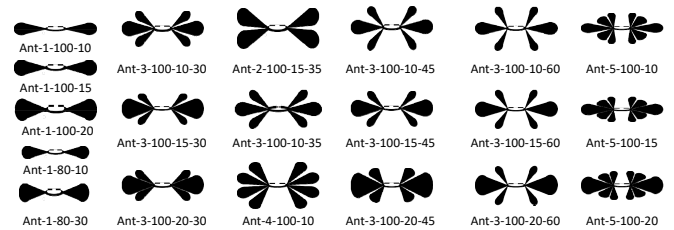
Fig. 4: Antenna shape and dimensions. For Ant-3-100-15-45, the number of lobes is 3, antenna length d_{ant} is 100 mm, height h_{ant} is 15 mm, and the angle α of the side lobes 45°.
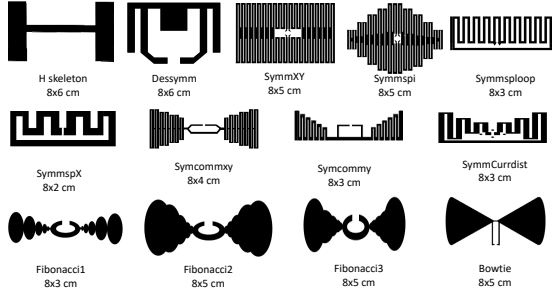
Fig. 5: Benchmark RFID antenna designs. H skeleton and Bowtie were proposed in [19] and [20], respectively.

at $\beta \geq 0°$.

Based on existing literature, we consider the meander line antenna pattern to begin our investigation into tag design for the thermal transfer printing method. As discussed in [10], the meander line functions as a transmission line, making it easier to adjust the impedance of the antenna. Our preliminary investigation into commercial tag prototypes, outlined in Figure 5 shows that the meander line antenna tested using our method of fabrication does not provide sufficient read range. We discover that a multi-lobe antenna, in which the lobes are all connected through a inner loop as shown in Figure 1, provides better read range performance for passive RFID tags than several commercial designs, including the meander line antenna.

Inner Loop. Through our experiments, we observe that the inner loop dimensions affect the impedance of the antenna. Changes to the values of parameters d_{in} and d_{out} can result in significant changes to the performance of the selected antenna. Simulation of tags across the tested ranges of d_{in} and d_{out} with similar lobe geometry show large variations in the current distribution and impedance around the chip box. We find that, similar to the meander line approach discussed in II, the inner loop geometry is a key design parameter for both balancing the antenna current distribution as well as tuning the antenna impedance to match the selected chip. We identify the optimal inner loop geometry based on the chip we are using for this experiment, which is Higgs 3 IC with an impedance of 50 ω.

Antenna Printing. To print the new RFID antenna, we first draw the antenna using graphic design software and save as high-resolution PDF. The antenna design is then printed using the Zebra ZT610 thermal transfer printer as shown in Fig. 3 with aluminum ribbon produced by ARMOR-IIMAK. After the tag is printed, the chip is manually attached to the chip box on the printed antenna. Figure 2(a) shows the lab setup and the major devices and facilities required for the RFID development process. Figure 2(b) shows the tools and equipment used for tag prototyping. In order to finish the tag manually, a digital optical microscope is used to place the small chips accurately using a vacuum pen in the chip box to prevent short circuiting.

Chip Attachment. Since the chip cannot be soldered onto the printed Aluminum ribbon, we investigate two approaches to chip attachment which provide minimum contact impedance so that the calculated antenna impedance can be maintained.

Fig. 6: Snapshot of experiments. (Left) printed antenna Ant-5-100-10; (Right) read range measurement.

The first approach is dry inlay approach using double-sided conductive adhesive tape. The tape is laid directly on the edges of the antenna chip box, and the chip is attached on top. The second approach is a wet inlay approach using silver epoxy 8330D-19G. The curing process for the epoxy is accelerated significantly using an oven or a heat press. In this work, we apply a heat press of 75°C to the epoxy for 45 min and let it cure for another 15 min in the room temperature. In both processes, an air cavity is introduced in the chip box during tag prototyping by manually creating a small cavity in the substrate using a knife. This can significantly improve the performance of the resulting RFID tag and can help avoid short circuits for both wet and dry inlay methods. While manual tag construction is time-consuming for prototype tags, the rapid and reliable nature of the thermal transfer printing method has been shown to enable ready integration with precision manufacturing processes [29].

V. EXPERIMENTAL EVALUATION

We test the performance of the manufactured RFID tags in terms of impedance and read range when operating at frequency 915 MHz using the TURCK uGrokit UHF handheld reader to collect data. This reader is compatible with most smartphones and relies on an iOS/Android application interface to operate the reader, communicate with the chip,m and change its EPC value. In our experiments, we consider 13 benchmark designs for performance comparison, which are shown in Figure 5. Among these, H Skeleton [19] and Bowtie [20] are two popular tags. Figure 6 shows a snapshot of the experiments.

With the testing on some of the popular designs as well as our designs, we modify commercial designs and update them with our tested dimensions of d_{ant}, h_{ant} and the corresponding inner loop dimensions. We found that the inner loop dimension d_{in} is an important design factor due to its impact on the current distribution of the antenna.

Impedance Measurement. As discussed in Section IV, an important criteria of RFID antenna design is the impedance match between the selected IC and the antenna element. The objective of impedance matching is to improve the radiation efficiency of the backscatter signal. Most ASICs designed for commercial tags have an impedance of 50 or 50 $\pm Xj$ ohms. In practice, the antenna impedance should be as close to 50 $\pm Xj$ as possible. While we can estimate the impedance of an antenna design during simulation, we validate this estimate prior to chip attachment to ensure expected tag performance. We measure the impedance of the printed antennas using Vector Network Analyzer (VNA) Agilent 8753ES, as shown

TABLE I: Range, impedance, and read times of benchmark tags compared with several proposed antenna designs, which have been listed in bold.

Name	Range (m)	Time (s)	Impedance
H skeleton	0	∞	64- 12j
Dessymm	0	∞	59-8j
SymmXY	0.4	7	56-7j
Symmspi	0.6	2	54-10j
Symmsloop	0.7	2	53-4j
SymmspX	0.9	3	49-13j
Symcommy	2	7	50.5-5j
SymmCurrdist	2	1	51-4j
Fibonacci1	2	7	-
Fibonacci2	3	7	-
Fibonacci3	3	7	-
Bowtie	4	10	-
Ant-1-80-30	6	5	50-3.4j
Ant-1-80-10	9	5	50-3j
Ant-1-80-15	10	5	50-2j
Ant-1-100-15	16.3	5	50-2j

TABLE II: Range of Ant-1-d_{ant}-h_{ant} for different configurations of d_{ant} and h_{ant}.

Dimension d_{ant} x h_{ant} (cm)	Range (m)
8x5	5
8x3	7
8x1	12.5
10x3	7.5
10x2	12.5
10x1.5	14
10x1	16.3

in Figure 2(a). To this end, we design a custom probe, based on which the antenna can be interfaced with the VNA for impedance measurement. The VNA needs to be calibrated to simulate the attached chip and measure the impedance across the chip box.

Read Range Measurements. The read range of each antenna is evaluated using a COTS handheld RFID reader as discussed in Section IV. The reader is connected to a smartphone device, which is held at the start of a measuring tape. The tag was held aloft at the other end, with all sources of RFID interference (e.g. cell phones) removed from the testing environment. An example of the measurement process is shown in Figure 6.

Read range, read time, and impedance measurements for selected benchmark and commercial tag designs as well as several novel designs are presented in Table I. The proposed antenna designs, $Ant - 1 - d_{ant} - h_{ant}$, are shown to significantly outperform all other tested tags. The read time for the proposed tags is shown to be consistent as well, and
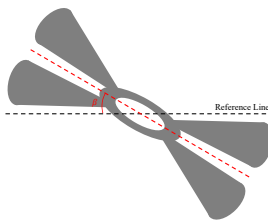
Fig. 7: Orientation angle β.
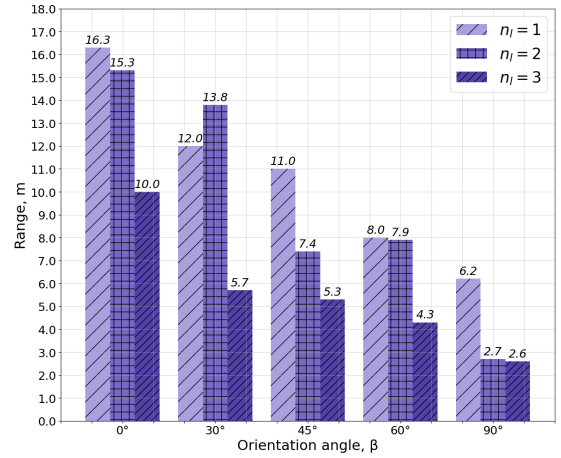
Fig. 8: Measurement of range, width, and orientation angle β for Ant-n_l-100-10 for different number of lobes, n_l.

comparable to the average read time of the other considered tags. For some antenna designs, such as H skeleton and Dessymm, we are unable to receive any backscatter signal regardless of read time. Other designs provide very low read range, i.e. < 1 m. As discussed in Section IV, matched impedance of 50 Ω between the antenna chip box and the chip is shown to be crucial for overall tag performance. We are unable to collect conclusive impedance measurements for $Fibonacci1$, $Fibonacci2$, $Fibonacci3$ and $Bowtie$ antennas.

Read range measurements for different combinations of antenna width d_{ant} and height h_{ant} are reported in Table II. This data demonstrates the relationship between the selected wavelength λ and the expected optimal tag dimension of $d_{ant} \geq \lambda/4$, as well as the effect of varying h_{ant} under this constraint. It is shown that a read range of 16.3 m can be achieved following this constraint, while minimizing h_{ant} to maintain optimal current distribution.

Performance for varying number of lobes n_l in terms of read range at various values of β is reported in Figure 8. Modification to the number of lobes is shown to have significant impact on both the current distribution of the tag, as well as the radiation pattern. The decrease in range with respect to the increase in the number of lobes is significant, with a reduction by over 33% in the best case for $n_l = 3$. Due to the strict relationship between current distribution and backscatter signal strength, we observe that considering fixed antenna dimensions, minimizing n_l provides the optimal read range.

Table III reports the maximum achievable range of antenna Ant-3-100-h_{ant}-α for various combinations of angle α and reader orientation β, which is shown in Figure 7. For brevity we limit our discussion to the four data points which indicate the optimal case for both β and h_{ant} for each antenna. We observe a very strong correlation between these variables, indicating that increasing the lobe angle can improve the rotational performance of the tag at the cost of reduced

TABLE III: Measurement of achievable range based on tag width and orientation angle for Ant-3-100-h_{ant}-α for different lobe angle α.

Lobe Angle (α)	Orientation Angle(β)	Range (m)
30°	30°	8
35°	45°	11
45°	50°	10
60°	60°	6

TABLE IV: Read range performance of for antenna Ant-3-100-h_{ant}-α for various values of t_{out} and α.

Thickness t_{out} (cm)	Angle α	Range (m)
1	30°	11.6
	35°	12.5
	45°	11
	60°	8
1.5	30°	8.5
	35°	11
	45°	11
	60°	10
2	30°	4
	35°	9
	45°	6
	60°	5

TABLE V: Maximum horizontal backscatter beam width for varying number of lobes.

Number of lobes n_l	Width
1	360°
2	180°
3	90°
4	30°
5	30°

performance at $\beta = 0$. As a result, we can consider α to be a design parameter which can address β defined by application-specific requirements during the antenna design process.

Figure 9 shows the change in lobe thickness with change in angle α for a 3-lobe design Ant-3-100-15-α. We observe in Table III that for the 3 lobe tag, optimum angle is 35° for a lobe height of 1 cm. To understand the effect of height and angle, we consider these variations in Figure 9. We observe that fewer, thinner lobes provide a significantly improved read range of up to 14 m compared to 5 m with many wider lobes.

Table IV demonstrates the relationship between lobe thickness and angle between lobes for antenna Ant-3-100-10-35. We observe similar results to Figure 9, which indicate that thinner lobes will provide better read range. Interestingly, we observe maximum read range for all configurations at $\alpha = 35°$. This implies that slight separation between lobes, and therefore correlation between n_l and h_{ant}, is important for uniform current distribution around the inner loop of the tag, while minimal or excessive lobe separation reduces performance overall. This is supported by our findings in Figure 8, in which n_l is varied without changing h_{ant}.

The results presented in Table V indicate the relationship between number of lobes n_l and the width of the region in which the backscatter signal can be recovered by the receiver. We observe that for $n_l = 1$, the proposed antennas demonstrate isotropic performance, while for increasing n_l, the proposed antennas rely on a more strict orientation of the reader during operation.

A popular commercial tag, Bowtie, is an effective tag that has been referenced in much of the related literature. The tag has been designed using T-match stubs to match the impedance of the chip as referenced in [20]. In our design, our inner loop consists of dimensions d_{in}, d_{out}, t_{in} to match the impedance of the Higgs 3 IC. Figure 10 gives a comparison of the commercially available tag with our design. All three tags are printed using thermal transfer technique on paper with ZT610, integrated with Higgs 3, tested on Turck UGrokit RFID reader in the same environment. The first design, proposed in [20], provides a maximum read range of 4.5 m. The variation with matched impedance, Bowtie with Ant loop, represents the antenna with dimensions as stated in [20] modified with the inner loop from the Ant-series designed by our lab. The loop increases the read range significantly with an average range of 8 m, compared with Ant-1-100-15 which has a novel read range of 16.3 m.
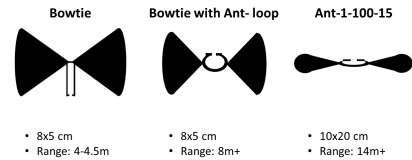
Fig. 10: Bowtie antenna and Ant-loop variation next to our proposed antenna design.

VI. CONCLUSIONS AND FUTURE WORK

We have presented a new RFID antenna design with multiple lobes based on conductive thermal transfer printing. The key antenna design parameters have been discussed. We have printed the novel antenna design using conductive Aluminum ribbon on PET-coated paper operating at 915 MHz frequency, and evaluated the performance of the new antenna

Fig. 9: Range measurement for Ant-3-100-h_{ant}-α considering different lobe thickness t_{out} and number of lobes.

by comparing it with 13 existing benchmark antennas through an extensive experimentation campaign. We have found that several of the proposed antenna designs achieve state-of-the-art read range during operation in the UHF band, surpassing many existing benchmarks. Future research directions include i) designing chipless RFID tags based on conductive thermal transfer printing technology; and ii) joint tag and reader design based on advanced signal processing and communication techniques such as massive multiple-input multiple-input (MIMO).

REFERENCES

[1] S. Aghili and H. Mala, "Security analysis of an ultra-lightweight RFID authentication protocol for m-commerce," *International Journal of Communication Systems*, vol. 32, no. 3, p. e.3837, December 2018.

[2] A. Alwadi, A. Gawanmeh, S. Parvin, and J. Al-Karaki, "Smart Solutions for RFID based Inventory Management Systems: A Survey," *Scalable Computing: Practice and Experience*, vol. 18, no. 4, pp. 347–360, November 2017.

[3] A. Abugabah, N. Nizamuddin, and A. Abuqabbeh, "A review of challenges and barriers implementing RFID technology in the Healthcare sector," *Procedia Computer Science*, vol. 170, pp. 1003–1010, January 2020.

[4] N. Khalid, R. Mirzavand, and A. Iyer, "A survey on battery-less RFID-based wireless sensors," *Micromachines*, vol. 12, no. 7, p. 819, July 2021.

[5] W. yang, X. Cheng, Z. Guo, Q. Sun, J. Wang, and C. Wang, "Design, fabrication and applications of flexible RFID antennas based on printed electronic materials and technologies ," *Journal of Materials Chemistry C*, vol. 11, no. 2, pp. 406–425, 2023.

[6] M. U. Ali Khan, R. Raad, J. Foroughi, F. E. Tubbal, and J. Xi, "Novel bow-tie chip-less rfid tag for wearable applications," in *2019 19th International Symposium on Communications and Information Technologies (ISCIT)*, 2019, pp. 10–13.

[7] K. S. Rao, V. Nikitin, and S. F. Lam, "Antenna Design for UHF RFID Tags: A Review and a Practical Application," *IEEE Transactions on Antennas and Propagation*, vol. 53, no. 12, pp. 3870 – 3876, December 2005.

[8] G. Marrocco, "The art of UHF RFID antenna design: impedance-matching and size-reduction techniques," *IEEE Antennas and Propagation Magazine*, vol. 50, no. 1, pp. 66–79, April 2008.

[9] A. Toccafondi and P. Braconi, "Compact load-bars meander line antenna for uhf rfid transponder," in *2006 First European Conference on Antennas and Propagation*. IEEE, 2006, pp. 1–4.

[10] G. Marrocco, "Gain-optimized self-resonant meander line antennas for rfid applications," *IEEE Antennas and Wireless Propagation Letters*, vol. 2, pp. 302–305, 2003.

[11] T. J. Warnagiris and T. J. Minardo, "Performance of a meandered line as an electrically small transmitting antenna," *IEEE Transactions on Antennas and Propagation*, vol. 46, no. 12, pp. 1797–1801, 1998.

[12] A. Motroni, F. Bernardini, A. Buffi, P. Nepa, and B. Tellini, "A UHF-RFID multi-antenna sensor fusion enables item and robot localization," *IEEE Journal of Radio Frequency Identification*, vol. 6, pp. 456–466, April 2022.

[13] R. Jouali *et al.*, "Design of an Analog RFID-Based Tag Antenna with Opened Circuited L-Shaped Stubs for Applications in Localization," *Electronics*, vol. 11, no. 7, pp. 1027–1042, March 2022.

[14] H. Zhu, Y. C. A. Ko, and T. T. Ye, "Impedance measurement for balanced UHF RFID tag antennas," in *2010 IEEE Radio and Wireless Symposium (RWS)*, New Orleans, LA, USA, March.

[15] Ansys. 3D Electromagnetic Field Simulator for RF and Wireless Design. (2023). [Online]. Available: https://www.ansys.com/products/electronics/ansys-hfss

[16] C. Cai, W. Hong, L. Deng, and S. Li, "Impedance measurement of rfid tag antenna based on different methods," in *2017 IEEE 5th International Symposium on Electromagnetic Compatibility (EMC-Beijing)*. IEEE, 2017, pp. 1–4.

[17] B. Walker, "Make accurate impedance measurements using a vna," *Microw. RF*, pp. 30–36, 2019.

[18] J. D. Griffin, *High-frequency modulated-backscatter communication using multiple antennas*. Georgia Institute of Technology, 2009.

[19] G. Q. Luo, Z. Z. Song, X. H. Zhang, and X. P. Hu, "Millimeter wave on chip antenna using dogbone shape artificial magnetic conductor," *International Journal of Antennas and Propagation*, vol. 2013, 2013.

[20] Y. Amin, S. Prokkola, B. Shao, J. Hållstedt, Q. Chen, H. Tenhunen, and L.-R. Zheng, "Low cost paper based bowtie tag antenna for high performance uhf rfid applications," in *Proc. of Nanotech Conference & Expo*, 2009, pp. 538–541.

[21] J. Gigac, M. Fišerová, and S. Hegyi, "Comparison of thermal transfer and inkjet printing of uhf rfid tag antennas on paper substrates," *Wood Research*, vol. 66, no. 1, pp. 71–84, 2021.

[22] C. Luo *et al.*, "Textile UHF-RFID Antenna Embroidered on Surgical Masks for Future Textile Sensing Applications," *IEEE Transactions on Antennas and Propagation*, vol. 70, no. 7, pp. 5246–5253, January 2022.

[23] F. Chietera *et al.*, "Laser-Induced Graphene, Fused Filament Fabrication, and Aerosol Jet Printing for Realizing Conductive Elements of UHF RFID Antennas," *IEEE Journal of Radio Frequency Identification*, vol. 6, pp. 601–609, April 2022.

[24] Z. Lopez, Z. Akhter, and A. Shamim, "3D printed RFID tag antenna miniaturized through volumetric folding and slow-wave structures," *IEEE Journal of Radio Frequency Identification*, vol. 6, pp. 164–175, February 2022.

[25] A. C. Durgun, C. A. Balanis, C. R. Birtcher, and D. R. Allee, "Design, simulation, fabrication and testing of flexible bow-tie antennas," *IEEE Transactions on Antennas and Propagation*, vol. 59, no. 12, pp. 4425–4435, 2011.

[26] K. Dziadak-Curtis, B. Kumar, and J. Sommerville, "Rfid in the built environment: Buried asset locating systems," in *Workshop of the European Group for Intelligent Computing in Engineering*, vol. 4200, 01 2006, pp. 153–162.

[27] C. Occhiuzzi, S. Cippitelli, and G. Marrocco, "Modeling, Design, and Experimentation of Wearable RFID Sensor Tag," *IEEE Transactions on Antennas and Propagation*, vol. 58, no. 8, pp. 2490–2498, August 2010.

[28] J. Wang, "Spiral antennas in RFID and their size reduction and performance enhancement," in *International Workship on Anti-Counterfeiting, Security and Identification*, Xiamen, China, April 2007.

[29] S. Duan, J. Wang, Y. Lin, J. Hong, Y. Lin, Y. Xia, Y. Li, D. Zhu, W. Lei, W. Su, B. Wang, Z. Cui, W. Yuan, and J. Wu, "Highly durable machine-learned waterproof electronic glove based on low-cost thermal transfer printing for amphibious wearable applications," *Nano Research*, pp. 1–10, December 2022.